

Luminescence Studies of $\text{Sr}_2\text{MgSi}_2\text{O}_7:\text{Eu}^{2+}$, Dy^{3+} Phosphor prepared by Solid State Reaction Method

^aIshwar Prasad Sahu*, ^aD. P. Bisen, ^aNameeta Brahme, ^aRaunak Kumar Tamrakar

^aSchool of Studies in Physics & Astrophysics, Pt. Ravishankar Shukla University, Raipur (C.G.)
Pin Code - 492010, India

^bDepartment of Applied Physics, Bhilai Institute of Technology Durg (C.G.)
Pin Code - 491001, India

*Corresponding author Email Id: ishwarprasad1986@gmail.com

Abstract

Europium and dysprosium doped $\text{Sr}_2\text{MgSi}_2\text{O}_7:\text{Eu}^{2+}$, Dy^{3+} was prepared by the high temperature solid state reaction method. The prepared phosphor was characterized by X-ray diffractometer (XRD), energy dispersive x-ray spectroscopy (EDS) and fourier transform infrared (FTIR) spectroscopy techniques. The crystal structure of sintered phosphor was an akermanite type structure which belongs to the tetragonal crystallography with space group $P4_21m$, this structure is a member of the melilite group and forms a layered compound. EDS spectrum confirmed the present elements in the phosphor. The thermoluminescence (TL) glow were measured for various γ -dose. Initially, TL intensity increased with increasing γ -dose, but after specific γ -dose (10 Gy), TL intensity decreased. Under the ultraviolet excitation, the emission spectra of $\text{Sr}_2\text{MgSi}_2\text{O}_7:\text{Eu}^{2+}$, Dy^{3+} phosphor are composed of a broad band peaking at 470 nm, belonging to the $4f^65d^1 \rightarrow 4f^7$ transition. Decay graph indicated that this phosphor also contains fast decay and slow decay process. The mechanoluminescence (ML) intensities of $\text{Sr}_2\text{MgSi}_2\text{O}_7:\text{Eu}^{2+}$, Dy^{3+} phosphor are proportionally increased with the increasing the impact velocity of the mechanical load, which suggests that this phosphor can be used as sensors to detect the stress of an object.

Keywords: Akermanite; γ – Irradiated; Photoluminescence; CIE color coordinates; piezo-electricity.

Introduction

In the last decade, aluminate based phosphors MA_2O_4 (M= Ca, Sr, Ba) doped with rare earth ions (Eu, Dy) have attracted more interest due to their excellent properties such as high brightness, no radiation, long duration of afterglow, excellent photo resistance and environmental stability. However, such properties of these phosphors may be decreased significantly after soaking in the water for several hours, which limited their application in the pigments, paints and other fields [1-4].

Alkaline earth silicates based phosphors doped with Eu^{2+} and trivalent rare earth ions [$\text{M}_2\text{MgSi}_2\text{O}_7:\text{Eu}^{2+}$, R^{3+} (M = Sr, Ca, Ba; R = Nd, Dy, Tm) are useful luminescence hosts having a stable crystal structure with high physical and chemical stability. Silicate based phosphors possess strong resistance of water and good thermal stability. Furthermore, the starting materials for the synthesis of such silicates were abundant and cheap [5-8]. Alkaline earth silicates based phosphors shows the property of long afterglow. Therefore the silicate host is of great interest for material scientist in the application of long afterglow phosphors.

Long afterglow phosphors are a special kind of luminescent material with long persistent phosphorescence which can absorb light, store energy, and release energy as visible light following excitation. Moreover, these materials have persistent phosphorescence lasting for several hours at room temperature. In recent years, these materials have drawn more and more attention because of their diverse commercial applications in many fields such as traffic

signs, textile painting, emergency signs, watches and clocks, optical memory, imaging storage and so on [9-13].

In general, the afterglow of phosphors is attributed to traps which are associated with lattice defects in the host material. When phosphors are excited by UV light, a great number of holes and electrons are generated. Some free holes and electrons are trapped at trapping centers. After the removal of excitation, the trapped carriers are thermally released and they migrate in the valence or conduction bands, and then recombine with opposite charges, accompanied with light emission at luminescent centers [14-15].

In the present paper, we report the synthesis of distrontium magnesium disilicates ($\text{Sr}_2\text{MgSi}_2\text{O}_7$) doped with Eu^{2+} and co-doped Dy^{3+} phosphor by the high temperature solid state reaction method under a weak reducing atmosphere. The study of the structural characterization was investigated on the basis of X-Ray Diffraction (XRD), Energy Dispersive X-Ray Spectroscopy (EDS), Fourier Transform Infrared spectroscopy (FTIR) techniques. Luminescent properties were also investigated on the basis of thermoluminescence (TL), TL spectra, photoluminescence (PL), long afterglow, mechanoluminescence (ML) and ML spectra.

Experimental Synthesis

The powder samples of $\text{Sr}_2\text{MgSi}_2\text{O}_7:\text{Eu}^{2+}$, Dy^{3+} phosphor was prepared by the high temperature solid state reaction method. Strontium carbonate [SrCO_3 (99.90%)],

magnesium oxide [MgO (99.90%)], silicon di-oxide [SiO₂ (99.99%)], europium oxide [Eu₂O₃ (99.99%)] and dysprosium oxide [Dy₂O₃ (99.99%)], all of analytical grade, were employed in this experiment. 0.1mol% of boric acid [H₃BO₃ (99.99%)] was added as flux. Initially, the raw materials were weighed according to the nominal compositions of Sr₂MgSi₂O₇:Eu²⁺, Dy³⁺ phosphor, then the powders were mixed and milled thoroughly for 2 hour using the agate mortar and pestle. The grinded sample are placed in an alumina crucible and subsequently fired at 1200°C for 3 hours in a weak reducing atmosphere, generated with the help of activated charcoal. At last the nominal compounds were obtained after the cooling down of the programmable furnace.

Solid state reaction method is the most common and one of the simplest ways to prepare silicate materials. This method is commonly used in both industry and the laboratory. Therefore, the samples in the current study were produced by bulk materials synthesis using the conventional solid state reaction method [16].

Characterization Techniques

The crystal structure of the prepared Sr₂MgSi₂O₇:Eu²⁺, Dy³⁺ phosphor was characterized by powder XRD analysis. Powder XRD pattern has been obtained from Bruker D8 advanced X-ray powder diffractometer and the data were collected over the 2θ range 10°-80°. X-rays were produced using a sealed tube (CuKα) radiation source and the wavelength of X-ray was (1.54060 Å). The X-rays were detected using a fast counting detector based on Silicon strip technology (Bruker LynxEye detector). The crystal structure of the prepared sample was verified with the help of Joint Committee of Powder Diffraction Standard Data (JCPDS) file. (JCPDS: 75-1736). An Energy dispersive X-ray spectroscopy (EDS) was used for the elemental analysis of the prepared phosphor. The TL glow curves were recorded with the help of TLD reader 1009I by Nucleonix (Hyderabad, India Pvt. Ltd.). The excitation and emission spectra were recorded on a Shimadzu (RF 5301-PC) spectrofluorophotometer using the Xenon lamp (365 nm) as excitation source when measuring. The color chromaticity coordinates were obtained according to Commission International de l'Eclairage (CIE) 1931. The ML measurement was observed by the home made lab system comprising of RCA-931A photomultiplier tube (PMT). The ML glow curve can be plotted with the help of SM-340 application software installed in a computer attached with the storage oscilloscope [17]. The TL and ML spectrum was recorded with the help of different band pass interference (400–700 nm) filters. All measurements were carried out at the room temperature.

Results and discussion

XRD analysis

The crystal structure of the prepared phosphor was analyzed by the XRD. The position and intensity of diffraction peaks of the Sr₂MgSi₂O₇:Eu²⁺, Dy³⁺ phosphor was consistent with that of the powder diffraction file of International Center for Diffraction Database (ICDD: 75-1736) [19].

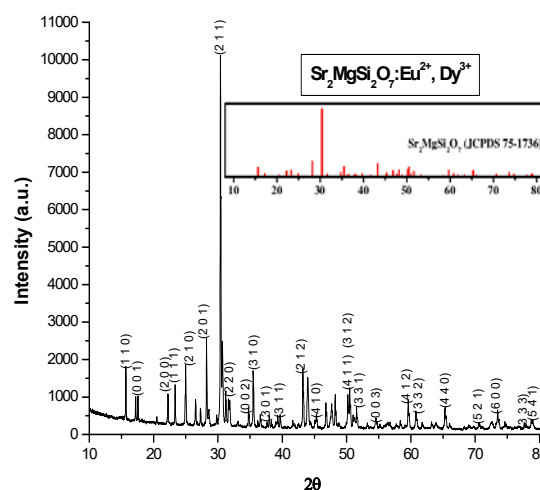


Fig. 1 XRD pattern of Sr₂MgSi₂O₇:Eu²⁺, Dy³⁺ phosphor

Fig.1 displays the XRD pattern of the prepared Sr₂MgSi₂O₇:Eu²⁺, Dy³⁺ phosphor, it can be concluded that the prepared sample was chemically and structurally Sr₂MgSi₂O₇. The crystal structure of the Sr₂MgSi₂O₇:Eu²⁺, Dy³⁺ phosphor was an akermanite type structure which belongs to the tetragonal crystallography with space group P4₂m, this structure is a member of the melilite group and forms a layered compound. The small amount of impurity did not change the crystal structure of the sintered phosphor. The radius of Eu²⁺ (1.12 Å) and Dy³⁺ (0.99 Å) are very close to that of Sr²⁺ (about 1.12 Å) rather than Mg²⁺ (0.65 Å) and Si⁴⁺ (0.41 Å). Therefore, the Dy³⁺ ions are expected to occupy the Sr²⁺ sites in the Sr₂MgSi₂O₇:Eu²⁺, Dy³⁺ phosphor.

Energy dispersive X-ray spectroscopy (EDS)

Fig. 2 shows the EDS spectra of Sr₂MgSi₂O₇:Eu²⁺, Dy³⁺ phosphor. The composition of the powder sample has been measured using EDS. Table 1 shows the compositional elements of Sr₂MgSi₂O₇:Eu²⁺, Dy³⁺ phosphor, which is compare with the standard element. EDS is a standard procedure for identifying and quantifying elemental composition of sample area as small as a few nanometers. Their appeared no other emissions apart from strontium (Sr), magnesium (Mg), silicon (Si), oxygen (O), europium (Eu) and dysprosium (Dy) in EDS spectra of the sample. In the spectrum intense peaks are present which confirm the

presence of elements in prepared $\text{Sr}_2\text{MgSi}_2\text{O}_7:\text{Eu}^{2+}, \text{Dy}^{3+}$ phosphor.

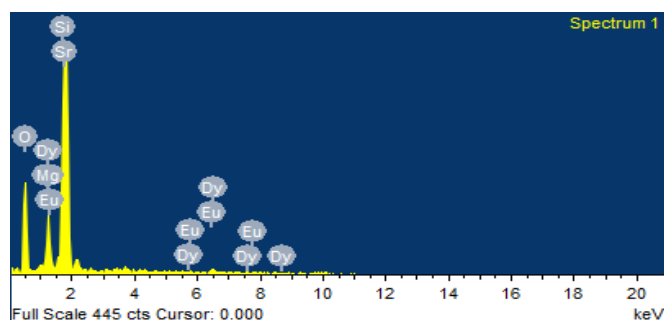


Fig. 2 EDX spectra of $\text{Sr}_2\text{MgSi}_2\text{O}_7:\text{Eu}^{2+}, \text{Dy}^{3+}$ phosphor

Table 1 Composite element of $\text{Sr}_2\text{MgSi}_2\text{O}_7:\text{Eu}^{2+}, \text{Dy}^{3+}$ phosphor

S.N.	Standard	Elements	Atomic(%)	Weight(%)
1	SiO_2	O K	33.91	63.85
2	MgO	Mg K	4.23	5.23
3	SiO_2	Si K	13.54	14.53
4	SrF_2	Sr L	47.21	16.18
5	EuF_3	Eu L	0.10	0.02
6	DyF_3	Dy L	1.00	0.18
Total			99.99	99.99

Fourier Transform Infrared Spectra (FTIR)

FTIR spectra have been widely used for the identification of organic and inorganic compounds. Spectroscopically, the middle infrared region is extremely useful for the study of organic and inorganic compounds. Fig. 3 shows the FTIR spectra of $\text{Sr}_2\text{MgSi}_2\text{O}_7:\text{Eu}^{2+}, \text{Dy}^{3+}$ phosphors in middle infrared region (4000 to 400 cm^{-1}). The wave-number of 3429.43 cm^{-1} is due to the O-H stretching mode. The O-H group around the 3429.43 cm^{-1} in sintered phosphors was might be due to presence of moisture through environment. The stretching around $\sim 1894.10, 1824.66, 1762.94 \text{ cm}^{-1}$ was assigned to CO_3^{2-} modes. The CO_3^{2-} modes (asymmetric stretching) around the 1900 to 1700 cm^{-1} in $\text{Sr}_2\text{MgSi}_2\text{O}_7:\text{Eu}^{2+}, \text{Dy}^{3+}$ phosphor is due the presence of carbonate [SrCO_3 (raw material)]. The free CO_3^{2-} ions has a D_{3h} symmetry (trigonal planar) and its spectrum is dominated by the band at 1900 to 1700 cm^{-1} . The vibration band of 1643.35 cm^{-1} are assigned due to the Mg^{2+} ions and bending of the sharp peaks in the region of 1485.19 cm^{-1} are assigned due to the bending of Sr^{2+} ions [20].

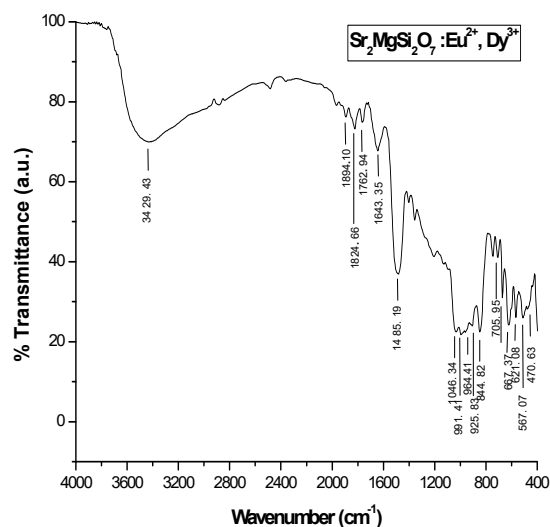


Fig. 3 FTIR Spectra of $\text{Sr}_2\text{MgSi}_2\text{O}_7:\text{Eu}^{2+}, \text{Dy}^{3+}$ phosphor

According to the crystal structure of $\text{Sr}_2\text{MgSi}_2\text{O}_7$, the coordination number of strontium can be 8 and 6. Therefore, Sr^{2+} can occupy two alternative lattice sites, the eight coordinated Sr^{2+} site [SrO_8 (Sr_1 site)] and the six coordinated Sr^{2+} site [SrO_6 (Sr_2 site)], and other two independent cations sites, namely Mg^{2+} [MgO_4], and Si^{4+} [SiO_4] also exist in the crystal lattice. Mg^{2+} and Si^{4+} cations occupy in the tetrahedral sites. Eu^{2+} ions can also occupy two alternative lattice sites with the coordination number of 8 [EuO_8 (Eu_1 site)] and 6 [EuO_6 (Eu_2 site)]. It's hard for Eu^{2+} ions to incorporate the tetrahedral [MgO_4] or [SiO_4] symmetry but it can easily incorporate octahedral [SrO_6] or hexahedral [SrO_8]. Another fact that supports that only Eu^{2+} ions is expected to replace Sr^{2+} in the $\text{Sr}_2\text{MgSi}_2\text{O}_7$, since the ionic radius of the of Eu^{2+} and Sr^{2+} species are close to a perfect match 1.12 \AA and 1.12 \AA respectively rather than Mg^{2+} (0.65 \AA) and Si^{4+} (0.41 \AA). Therefore, the Eu^{2+} ions are expected to occupy the Sr^{2+} sites in the $\text{Sr}_2\text{MgSi}_2\text{O}_7:\text{Eu}^{2+}, \text{Dy}^{3+}$ phosphor [21, 22].

In the presented spectrum the absorption bands of silicate groups were clearly evident. The Si-O-Si stretching modes for the silicate tetrahedral show infrared absorption bands, located at about $1046.34, 844.82, 705.95, 667.37,$ and 621.08 cm^{-1} . The characteristic band centered at approximately $991.41, 964.41, 925.83 \text{ cm}^{-1}$ is assigned to the Si-O stretching vibrations of the $\text{Si}(\text{Q}_2)$ tetrahedral and the group of bands at approximately $567.07, 470.63 \text{ cm}^{-1}$ correspond to the deformation of the TO_4 tetrahedral form as well as the Mg-O modes. (T = Si, Mg) [23, 24].

Thermoluminescence (TL)

Thermoluminescence (TL) is the emission of light from some solids commonly called phosphors, which can be observed when it is heated. The TL is observed under three conditions. Firstly, the phosphors must be either semiconductor or an insulator. Secondly, the material ability to energy store when exposure radiation. Thirdly, the luminescence emission is released by heating the material [25]. However, if the ionizing radiation is incident on a material, may be some of its energy absorbed, the material will store the energy with the release in the form of visible light when the material is heated. [26].

TL measurements provide information concerning the trap levels. The temperature dependence of the emission intensity is called the glow curve [27]. The excitation energy partly does the work of moving electrons to traps. Some of these electrons are trapped and locate themselves at a depth (activation energy E) below the conduction band. The radiation energy stored in the form of trapped electrons is released by raising the temperature of the material and the released energy is converted to luminescence [28].

Fig. 4 shows the TL glow curve of $\text{Sr}_2\text{MgSi}_2\text{O}_7:\text{Eu}^{2+}, \text{Dy}^{3+}$ phosphor with different γ dose (1, 5, 10 and 15 Gy) with a heating rate of 5°C s^{-1} . The TL glow curve peak were occurred at 65.82°C and these peak positions remains constant with different γ dose. From the TL glow curve, it is seen that, initially TL intensity increase with increasing γ dose. TL intensity are maximum for 10 Gy of γ dose, after that they start to decrease. The charge carrier density may have been increasing with increasing γ dose, but after specific dose of 10 Gy, the trap level may have started to be destroyed resulting in a decrease in TL intensity. The decrease in the charge carriers density may be a reason for the low TL intensity at higher γ dose (15 Gy).

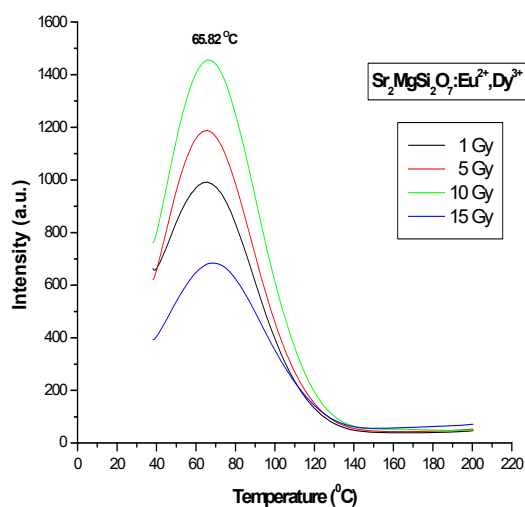


Fig. 4 TL glow curve of γ - irradiated $\text{Sr}_2\text{MgSi}_2\text{O}_7:\text{Eu}^{2+}, \text{Dy}^{3+}$ phosphor

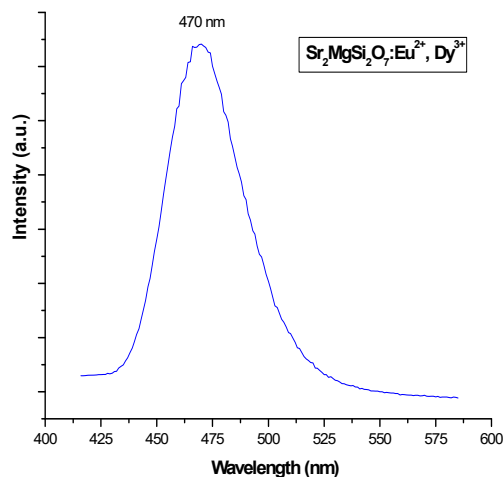


Fig. 5 TL spectra of $\text{Sr}_2\text{MgSi}_2\text{O}_7:\text{Eu}^{2+}, \text{Dy}^{3+}$ phosphor

Fig. 5 shows the TL emission spectra of $\text{Sr}_2\text{MgSi}_2\text{O}_7:\text{Eu}^{2+}, \text{Dy}^{3+}$ phosphor with a broad peak around 470 nm. This emission spectra confirms single isolated peak due to the formation of only one type of luminescence center is created due to the γ irradiation.

Photoluminescence (PL)

The excitation and emission spectra of $\text{Sr}_2\text{MgSi}_2\text{O}_7:\text{Eu}^{2+}, \text{Dy}^{3+}$ phosphor are shown in Fig. 6. Both of them are broadband spectra. The excitation broad band is due to transitions of $(4f^7)$ ground state to excited state $(4f^65d^1)$ [$4f^7 \rightarrow 4f^65d^1$] and emission broad band is due to transitions of excited state $(4f^65d^1)$ to ground state $(4f^7)$ [$4f^65d^1 \rightarrow 4f^7$] configuration were observed under the ultra violet excitation [29].

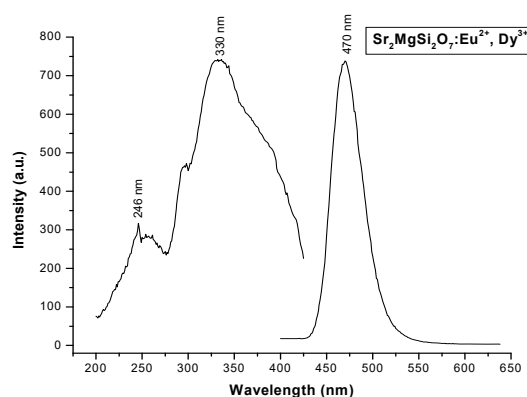


Fig. 6 Photoluminescence spectra of $\text{Sr}_2\text{MgSi}_2\text{O}_7:\text{Eu}^{2+}, \text{Dy}^{3+}$ phosphor

However, the Dy^{3+} emission peaks are found at around 460-480 nm (blue region) and 560-580 nm (yellow region) and special Eu^{3+} emission peak are found at the 590 nm (orange) and 613 nm (red region). In our experiments, there is no other emission due to Eu^{3+} , in the spectra, which implies that Eu^{3+} ions have been reduced as Eu^{2+} completely, and the co-doped Dy^{3+} is either weak or they transferred the absorbed energy to Eu^{2+} ions in crystal lattice [30].

CIE Chromaticity Coordinate

In general, color of any phosphor material is represented by means of color coordinates. The luminescence color of the samples were excited under 330 nm has been characterized by the CIE (Commission International de l'Eclairage) 1931 chromaticity diagram [31]. The emission spectrum of the $\text{Sr}_2\text{MgSi}_2\text{O}_7:\text{Eu}^{2+}, \text{Dy}^{3+}$ phosphor was converted to the CIE 1931 chromaticity using the photoluminescent data and the interactive CIE software (CIE coordinate calculator) diagram as shown in Fig. 7.

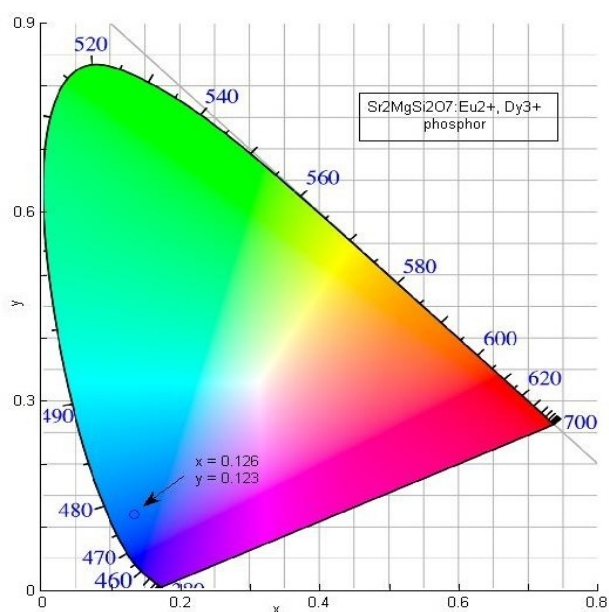


Fig. 7 CIE chromaticity diagram of $\text{Sr}_2\text{MgSi}_2\text{O}_7:\text{Eu}^{2+}, \text{Dy}^{3+}$ phosphor

Every natural color can be identified by (x, y) coordinates that are disposed inside the 'chromatic shoe' representing the saturated colors. Luminescence colors of $\text{Sr}_2\text{MgSi}_2\text{O}_7:\text{Eu}^{2+}, \text{Dy}^{3+}$ phosphor are placed in the blue ($x = 0.126, y = 0.123$), corners.

Long Afterglow (Decay)

Fig. 8 shows the typical decay curves of $\text{Sr}_2\text{MgSi}_2\text{O}_7:\text{Eu}^{2+}, \text{Dy}^{3+}$ phosphor. The initial afterglow intensity of the sample was high. The decay times of phosphor can be calculated by a curve fitting technique, and the decay curves fitted by the sum of two exponential components have different decay times.

$$I = A_1 \exp(-t/\tau_1) + A_2 \exp(-t/\tau_2) \quad (4)$$

where, I is phosphorescence intensity, A_1, A_2 are constants, t is time, τ_1 and τ_2 are decay times (in second) for the exponential components. Decay curves are successfully fitted by the equation (1) and the fitting curve result are shown in Table 1. The results indicated that this phosphor contains fast decay and slow decay processes [32].

The co-doped Dy^{3+} acts as trap centers in silicates that trap the electrons generated during the exposure of phosphor to excitation source. The mechanism of afterglow in silicate based phosphor has been explained by many researchers and may be elaborated as: on receiving exposure to excitation source, an electron of Eu^{2+} ($4f^7$) is promoted to the $4f^65d^1$ band followed by either direct or phonon assisted escape of the electron from Eu^{2+} to the host conduction band. The lattice defects close to the bottom of the host conduction band traps the electrons. Huge numbers of electrons are trapped by the traps assisted by Dy^{3+} at various depths making an important role of Dy^{3+} during the long afterglow. After the removal of excitation source, the captured electrons near the host conduction band released to the conduction band with thermal energy and consequent recombination of them with the emitting Eu^{2+} centers lead the persistent afterglow. Thus, the major cause for the afterglow is the number of electrons captured in the traps and its depth from the bottom of the conduction band of host material [33].

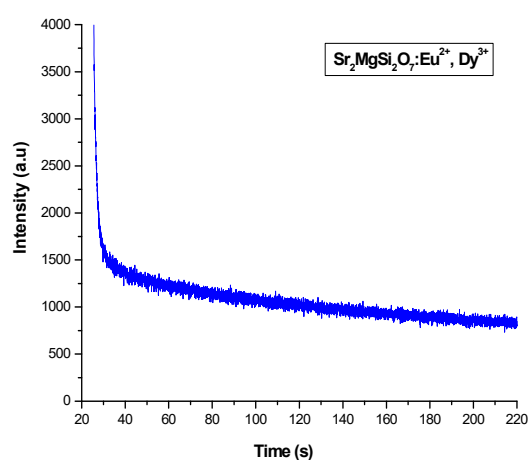


Fig. 8 Decay Curve of $\text{Sr}_2\text{MgSi}_2\text{O}_7:\text{Eu}^{2+}, \text{Dy}^{3+}$ phosphor

Table 1 Fitting results of the decay curves

Phosphor	τ_1 (s)	τ_2 (s)
$\text{Sr}_2\text{MgSi}_2\text{O}_7:\text{Eu}^{2+}, \text{Dy}^{3+}$	1.57	95.06

Mechanoluminescence (ML)

Mechanoluminescence (ML) is caused by mechanical stimuli such as grinding, cutting, collision, striking and friction. It is defect related phenomenon, associated with a trap involved process, in which electrons (or holes) dwell in the trap for some time and then recombine with the luminescence center either by travelling in the conduction band (or valence band) or by electron (or holes) tunneling. For ML materials, the recombination process is facilitated by the assistance of dislocation in the crystal [34]. In the recent past, intense ML materials have been prepared whose emission can be seen in daylight with naked eye and such materials are finding important applications in novel self-diagnosis systems, optical stress sensors, stress imaging devices, wireless fracture sensor systems and in damage sensors. The ML technique is much simpler, cheaper and more suited to the detection of fast crack than the conventional techniques, which involves complicated instrumentation. In the present ML studies, an impulsive deformation technique has been used. During the deformation of a solid, a great number of physical processes may occur within very short time intervals, which may excite or stimulate the process of photon emission [35]. It is seen that when moving piston is released at particular height, then the ML emission also takes place. When a load is applied to the phosphor, initially the ML intensity increases with time, attains a peak value and then decreases with time. Such a curve between the ML intensity and time of phosphors is known as ML glow curve [36].

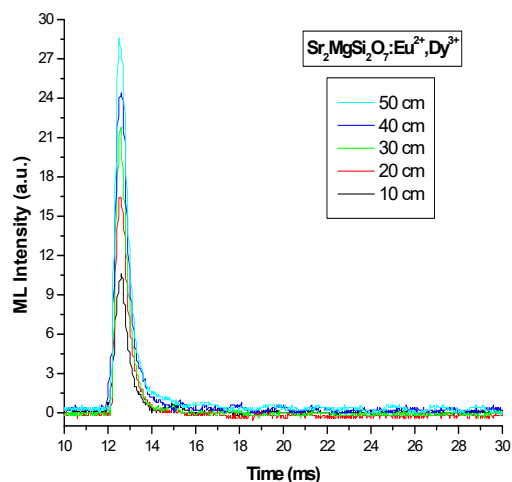


Fig. 9 ML intensity versus time curve of $\text{Sr}_2\text{MgSi}_2\text{O}_7:\text{Eu}^{2+}, \text{Dy}^{3+}$ phosphor

Fig. 9 shows that the characteristic curve between ML intensity versus time for different heights ($h = 10, 20, 30, 40, 50$ cm). The phosphor was fractured via dropping a load [moving piston] of particular mass (400 g) and cylindrical shape on the $\text{Sr}_2\text{MgSi}_2\text{O}_7:\text{Eu}^{2+}, \text{Dy}^{3+}$ phosphor. The velocity of the moving piston, holding the impact mass, could be changed, by changing the height through which it was dropped. Every time for the ML measurement, the quantity of $\text{Sr}_2\text{MgSi}_2\text{O}_7:\text{Eu}^{2+}, \text{Dy}^{3+}$ phosphor was kept constant (8 mg). When the moving piston was dropped onto the prepared phosphor at different height, light is emitted. The photon emission time is nearly 2 ms, when prepared $\text{Sr}_2\text{MgSi}_2\text{O}_7:\text{Eu}^{2+}, \text{Dy}^{3+}$ phosphor fractures. In these measurements, maximum ML intensity has been obtained for the 50 cm dropping height and ML intensity increases linearly with the increase in the falling height of the moving piston. The sintered $\text{Sr}_2\text{MgSi}_2\text{O}_7:\text{Eu}^{2+}, \text{Dy}^{3+}$ phosphor was not irradiated by any excitation source [37].

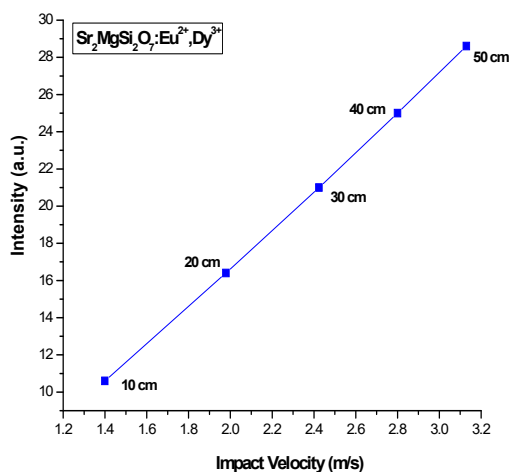


Fig. 10 ML intensity versus impact velocity curve of $\text{Sr}_2\text{MgSi}_2\text{O}_7:\text{Eu}^{2+}, \text{Dy}^{3+}$ phosphor

Fig. 10 shows the characteristics curve of ML intensity versus impact velocities for $\text{Sr}_2\text{MgSi}_2\text{O}_7:\text{Eu}^{2+}, \text{Dy}^{3+}$ phosphor. It is seen that, ML intensity increases linearly with increasing impact velocity [$\sqrt{2gh}$, (where “g” is the acceleration due to gravity and “h” is the height through which the load is dropped freely)] of the moving piston. The ML intensity of $\text{Sr}_2\text{MgSi}_2\text{O}_7:\text{Eu}^{2+}, \text{Dy}^{3+}$ phosphor increases linearly with increasing the mechanical stress.

ML spectra of $\text{Sr}_2\text{MgSi}_2\text{O}_7:\text{Eu}^{2+}, \text{Dy}^{3+}$ phosphors were recorded and shown in Fig. 11. The peak location of the ML spectra (470 nm), PL spectra (470 nm) and TL spectra (470 nm) of $\text{Sr}_2\text{MgSi}_2\text{O}_7:\text{Eu}^{2+}, \text{Dy}^{3+}$ phosphors consists of a broad emission band. As comparison of the ML, PL and TL spectra were found to be very similar in terms of shape of $\text{Sr}_2\text{MgSi}_2\text{O}_7:\text{Eu}^{2+}, \text{Dy}^{3+}$ phosphor, this implies that ML is emitted from the same emitting center of Eu^{2+} ions as PL and TL, which is also produced by the transition of Eu^{2+} ions between the excited states ($4f^65d^1$) to ground state ($4f^7$) is responsible for the blue ML emission [38].

When a mechanical stress, such as compression, friction, striking and so on, is applied on the sintered phosphors, piezoelectric field can be produced. Therefore, in such phosphors, the ML excitation may be caused by the local piezoelectric field near the impurities and defects in the crystals. During the impact on the material, one of its newly created surfaces gets positively charged and the other surface of the crack gets negatively charged [See Fig. 12]. Thus, an intense electric field of the order of $10^6 - 10^7$ Volt cm^{-1} is produced.

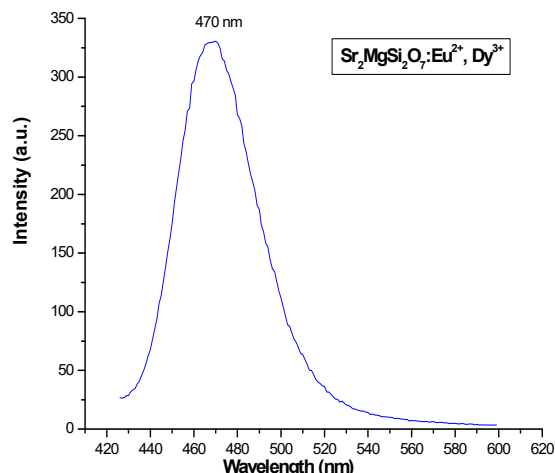


Fig. 11 ML spectra of $\text{Sr}_2\text{MgSi}_2\text{O}_7:\text{Eu}^{2+}, \text{Dy}^{3+}$ phosphor

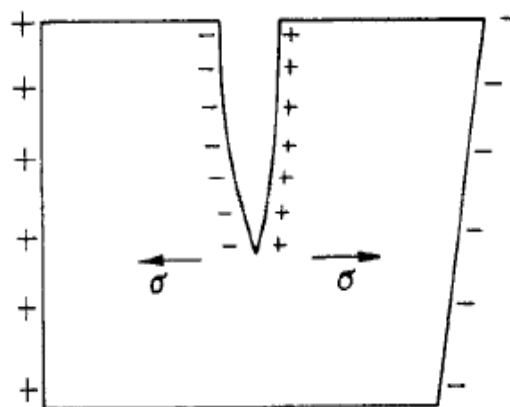


Fig. 12 Langevin model for the piezo-electrification induce phosphor

Under such order of electric field, the ejected electrons from the negatively charged surface may be accelerated and subsequently their impact on the positively charged surfaces may excite the luminescence center. Thus, depending on the prevailing conditions, recombination luminescence may be produced. For the impact velocity (v_0), the impact pressure P_0 will be equals to, $P_0 = Zv_0$, where Z is a constant. With increasing value of impact velocity, the depth of the trap will decrease, therefore, for the trap depth beyond a particular pressure the traps will be unstable and they will be de-trapped, in which the number of de-trapped electrons will increases with the increasing impact velocity. Thus, the ML intensity will increase proportionally with increasing value of impact velocity of the moving piston [39].

With the increasing impact velocity, more compression of the sample takes place, and therefore, more area of the

newly created surface takes place. Thus, the ML intensity will increase with increasing value of the impact velocity. It is to be noted that the stress near the tip of a moving crack is of the order of $\sigma/100 \approx 10^{10}$ dynes/cm² = 10^9 Newton/m² (where σ is the Young's modulus of the materials). Thus, a fixed charge density will be produced on the newly created surfaces and the increase in the ML intensity will primarily be caused by the increase in the rate of newly created surface area with increasing impact velocity. Moreover, the total ML intensity will also increase with impact velocity because more compression of the sample will create more surfaces with increasing impact velocity.

As the impact velocity increases, the impact pressure also increases leading to the increase in the electric field at local region which causes the decrease in trap depth. Hence the probability of de-trapping increases. From Fig. 10, it can be seen that with increasing impact velocity, ML intensity also increases linearly i.e., the ML intensity of Sr₂MgSi₂O₇:Eu²⁺, Dy³⁺ phosphor are linearly proportional to the magnitude of the impact velocity, which suggests that this phosphor can be used as sensor to detect the stress of an object [40].

CONCLUSION

Rare earth doped di-strontium magnesium di-silicate phosphor (Sr₂MgSi₂O₇:Eu²⁺, Dy³⁺) were prepared by the traditional high temperature solid state reaction method. The radius of Eu²⁺ (1.12 Å) and Dy³⁺ (0.99 Å) are very close to that of Sr²⁺ (about 1.12 Å) rather than Mg²⁺ (0.65 Å) and Si⁴⁺ (0.41 Å). Therefore, the Eu²⁺ and Dy³⁺ ions are expected to occupy the Sr²⁺ sites in the Sr₂MgSi₂O₇ host. EDS spectrum confirm the present elements in Sr₂MgSi₂O₇:Eu²⁺, Dy³⁺ phosphor. The TL glow curves of Sr₂MgSi₂O₇:Eu²⁺, Dy³⁺ phosphor showed that TL intensity has been increasing with increasing γ -dose, but after specific γ -dose (10 Gy) the density of charge carriers may have been destroyed resulting in a decrease in TL intensity. The prepared Sr₂MgSi₂O₇:Eu²⁺, Dy³⁺ phosphor would emit blue light with peak at 470nm. Sr₂MgSi₂O₇:Eu²⁺, Dy³⁺ phosphor emit the blue emission which was confirmed from the calculated CIE coordinates. The ML spectrum was compared with the PL and TL spectrum of the phosphor; a single sharp peak was observed which gives an indication of the presence of a single emission centre, which is produced by the transition of Eu²⁺ ions between the excited states (4f⁶5d¹) to ground state (4f⁷) is responsible for the blue emission. The dependence between ML intensities and loads are close to linearity, which suggests that these phosphor can be used as sensor to detect the stress of an object.

References:

1. Y. Chen, B. Liu, M. Kirm, Z. Qi, C. Shi, M. True, S. Vielhauer, G. Zimmerer, *J. Lumin.* 2006; 118: 70–78.
2. R. Yu, Y. Guo, L. Wang, H. M. Noh, B. K. Moon, B. C. Choi, J. H. Jeong, *J. Lumin.* 2014; 155:317-321.
3. B. Liu, C. Shi, M. Yin, L. Dong, Z. Xiao, *J. Alloys Compd.* 2005; 387: 65–69.
4. Yu Gong, Yuhua Wang, Ziqiang Jiang, Xuhui Xu, Yanqin Li, *Materials Research Bulletin* 2009; 44: 1916–1919.
5. Y. Kojima, M. Numazawa, T. Umegaki, *J. Lumin.* 2012; 132:2648-2652.
6. H. Liu, Y. Hao, H. Wang, J. Zhao, P. Huang, B. Xu, *J. Lumin.* 2011; 131:2422-2426.
7. I. P. Sahu, D. P. Bisen, Raunak Kumar Tamrakar, Ravi Shrivastava, *Res. Chem. Intermed.* (2015), DOI 10.1007/s11164-015-2120-4.
8. W. Pan, G. Ning, X. Zhang, J. Wang, Y. Lin, J. Ye, *J. Lumin.* 2008; 128: 1975-1979.
9. G.J. Talwar, C.P. Joshi, S.V. Moharil, S.M. Dhopte, P.L. Muthal, V.K. Kondawar, *J. Lumin.* 2009; 129: 1239-1241.
10. I. P. Sahu, *J Mater Sci: Mater Electron*, (2015), DOI 10.1007/s10854-015-3327-2.
11. I. P. Sahu, D. P. Bisen, N. Brhame, R.K. Tamrakar, R. Shrivastava *J Mater Sci: Mater Electron*, (2015), DOI 10.1007/s10854-015-3563-5.
12. C. N. Xu, T. Wantanabe, M. Akiyama, and X. G. Zheng, *Appl. Phys. Lett.* 1999; 74: 2414-2416.
13. N. Lakshminarasimhan, U.V. Varadaraju, *Mater. Res. Bull.* 2008; 43: 2946–2953.
14. F. Clabau, X. Rocquefelte, S. Jobic, P. Deniard, M.-H. Whangbo, A. Garcia, T. Le Mercier, *Chem. Mater.* 2005; 17: 3904–3912.
15. H. Wu, Y. Hu, G. Ju, L. Chen, X. Wang, Z. Yang, *J. Lumin* 2011;131: 2441-2445.
16. I P. Sahu, D. P. Bisen, N. Brahme, M. Ganjir, *Lumin. J. Biol. Chem. Lumin.* 2015; DOI 10.1002/bio.2900
17. I. P. Sahu, D. P. Bisen, N. Brahme, L. Wanjari, R. K. Tamrakar, *Res. Chem. Intermed.* (2015) DOI:10.1007/s11164-015-1929-1.
18. I. P. Sahu, D. P. Bisen, N. Brahme, R. Sharma, *Res. Chem. Intermed.* (2014) DOI 10.1007/s11164-014-1767-6.
19. JCPDS file number 75 - 1736, JCPDS International Center for Diffraction Data.
20. S. Basuna, G.F. Imbusch, D.D. Jiach, W.M. Yenc, *J. Lumin.* 104 (2003) 283.
21. M. A. Salim, R. Hussain, M. S. Abdullah, S. Abdullah, N. S. Alias, S. A. Ahmad Fuzi, M. N. Md Yusuf, K. M. Mahbor, *Solid State Science and Technology*, 2009; 17(2): 59-64.
22. I. P. Sahu, P. Chandrakar, R. N. Baghel, D. P. Bisen, N. Brahme, R.K. Tamrakar, *J. alloys. comp.* 2015; 649: 1329-1338.

23. I. P. Sahu, D. P. Bisen, N. Brahme, *Displays*, 2014; 35: 279 – 286.
24. G. T. Chandrappa, S. Ghosh, K. C. Patil, *J. Mater. Syn. Process.* 1999; 72-73.
25. Z. Yuan, C. Chang, D. Mao, W. Ying, *J. Alloys Compd.* 377(1–2), (2004) 268–271.
26. H. Kubo, H. Aizawa, T. Katsumata, S. Komuro, T. Morikawa, *J. Cryst. Growth.* 275(12) (2005) 1767–1771.
27. R. Chen, S.W.S. McKeever, World Scientific (1997).
28. H. N. Luitel, T. Watari, R. Chand, T. Torikai, M. Yada, *J. Mater.* 2013 (2013) 10.
29. T. Katsumata, R. Sakai, S. Komuro, T. Morikawa, *J. Electrochem. Soc.* 150 (2003) H111.
30. Z. Yuan, C. Chang, D. Mao, W. Ying, *J. Alloys Compd.* 377(1–2), (2004) 268–271.
31. CIE, International Commission on Illumination, Publication CIE no. 15, (E-1.3.1), 1931
32. I. P. Sahu, D. P. Bisen, N. Brahme, R. K. Tamrakar, *J. Radiat. Res. Appl. Sci.* 2015; 8: 104–109.
33. I. P. Sahu, D. P. Bisen, N. Brahme, *J. Radiat. Res. Appl. Sci.* 2015; (8)3: 381-388.
34. D.R. Vij, *Luminescence of Solids*, Plenum Press, New York (1998).
35. C. N. Xu, T. Wantanabe, M. Akiyama, and X. G. Zheng, *Appl. Phys. Lett.* 1999; 74: 1236 – 1238.
36. I. P. Sahu, D. P. Bisen, N. Brahme, *Displays* 2015; 38: 68 - 76.
37. I. P. Sahu, D. P. Bisen, N. Brahme, *Lumin. J. Biol. Chem. Lumin.* 2015; 30 (5): 526-532.
38. Zhang H, Yamada H, Terasaki N, Xu C N, *Int. J. Mod Phys B*, 2009; 23 (6-7): 1028 – 1033.
39. H. Zhang, H. Yamada, N. Terasaki, C.N. Xu, *Thin Solid Films* 518 610 – 613 (2009).
40. I. P. Sahu, D. P. Bisen, N. Brahme, R. K. Tamrakar, *J. Lumin.*, 2015; 167: 278-288.